Cerebral Cortex February 2013;23:460–476
doi:10.1093/cercor/bhs038
Advance Access publication February 23, 2012

Borders and Comparative Cytoarchitecture of the Perirhinal and Postrhinal Cortices in an F1 Hybrid Mouse

Stephane A. Beaudin[1,2], Teghpal Singh[1], Kara L. Agster[1,3] and Rebecca D. Burwell[1]

[1]Department of Cognitive, Linguistic, and Psychological Sciences, Brown University, Providence, RI 02912, USA

[2]Current address: Department of Microbiology and Environmental Toxicology, University of California, Santa Cruz 95064, USA

[3]Current address: Department of Psychiatry, University of North Carolina, Chapel Hill, USA

Address correspondence to Dr Rebecca D. Burwell, Department of Psychology, Brown University, 89 Waterman Street, Providence, RI 02912, USA. Email: rebecca_burwell@brown.edu.

We examined the cytoarchitectonic and chemoarchitectonic organization of the cortical regions associated with the posterior rhinal fissure in the mouse brain, within the framework of what is known about these regions in the rat. Primary observations were in a first-generation hybrid mouse line, B6129PF/J1. The F1 hybrid was chosen because of the many advantages afforded in the study of the molecular and cellular bases of learning and memory. Comparisons with the parent strains, the C57BL6/J and 129P3/J are also reported. Mouse brain tissue was processed for visualization of Nissl material, myelin, acetyl cholinesterase, parvalbumin, and heavy metals. Tissue stained for heavy metals by the Timm's method was particularly useful in the assignment of borders and in the comparative analyses because the patterns of staining were similar across species and strains. As in the rat, the areas examined were parcellated into 2 regions, the perirhinal and the postrhinal cortices. The perirhinal cortex was divided into areas 35 and 36, and the postrhinal cortex was divided into dorsal (PORd) and ventral (PORv) subregions. In addition to identifying the borders of the perirhinal cortex, we were able to identify a region in the mouse brain that shares signature features with the rat postrhinal cortex.

Keywords: acetylcholinesterase, Nissl, myelin, parvalbumin, Timm's stain

Introduction

Research on the neural bases of learning and memory has focused primarily on the hippocampus, but recent findings suggest that parahippocampal areas are critically involved. The perirhinal and postrhinal cortices provide the primary neocortical input to the hippocampus, both directly and indirectly through the entorhinal cortex. Beyond providing input to the hippocampus, these regions also have unique contributions to a number of learning and memory processes, including spatial memory, contextual memory, and object recognition (for review, see Eichenbaum 2000; Murray et al. 2000). With the development of new technologies for modifying the mouse genome, transgenic and gene-targeted mutant mice are becoming more widely used as models of memory and plasticity. Unfortunately, the neuroanatomy of the relevant brain structures in the mouse brain lags behind that of other models. To date, there has not been a detailed cytoarchitectonic analysis of the perirhinal area in the mouse brain, while the postrhinal cortex has been identified and described only in the briefest terms (Witter 2010).

Because of the lack of knowledge of corticohippocampal anatomy in the mouse, research in this system using mice too often relies on neuroanatomical findings in the rat. A review of the citations in recently published mouse stereotaxic atlases and an anatomy chapter revealed that the majority of the cited neuroanatomical studies were conducted in the rat (Hof et al. 2000; Dong 2008; Franklin and Paxinos 2008; Witter 2010). Yet, there are known species differences in corticohippocampal circuitry and function that could impact research on memory and learning using the mouse model. For example, mice and rats show differences in spatial learning abilities (Mizumori et al. 1982; Whishaw and Tomie 1996), and there are species differences in the organization of the perforant pathway a critical conduit for information to reach the hippocampus (van Groen et al. 2002). Species and strain differences in hippocampal morphology have been shown to correlate with spatial memory abilities. For example, size of mossy fiber terminal fields correlate with radial maze performance in inbred mouse strains (e.g., Schwegler and Crusio 1995). These studies highlight the importance of establishing reliable information about corticohippocampal structure and circuitry in the mouse brain.

As recently as a decade and a half ago, there was little agreement about the definition and borders of the cortical regions associated with the posterior rhinal fissure and surrounding the hippocampus in the rat brain (Burwell et al. 1995). We applied a comparative neuroanatomical approach to the analysis of these regions in the rat based upon what was known at the time in the monkey. The result was the parcellation of the area into the perirhinal cortex (PER), comprising areas 35 and 36, and the caudally adjacent postrhinal cortex (POR) (Burwell 2001). A similar situation exists now for the mouse, in that there is not much agreement about the boundaries and nomenclature for the regions in the mouse brain that are comparable to the PER and the POR in the rat brain. The critical questions are longstanding and are apparent in 2 historical definitions of the mouse neocortex (Fig. 1). Both Rose (1929) and Caviness (1975) defined 2 regions in the mouse brain that are roughly comparable to definitions of areas 35 and 36 in the rat brain. In both parcellations, the insular cortex is described as overlying the claustrum and the perirhinal areas arises at the caudal limit of the claustrum. The location of the rostral border, however, differs substantially, which may be due to strain differences. In addition, although overemphasized in Figure 1 because of differences in perspective, the dorsal boundaries also differ between the 2. Both Rose and Caviness used Brodmann's terminology; however, Rose (1929) employed the verbal designations, that is, "area perirhinalis" and "area

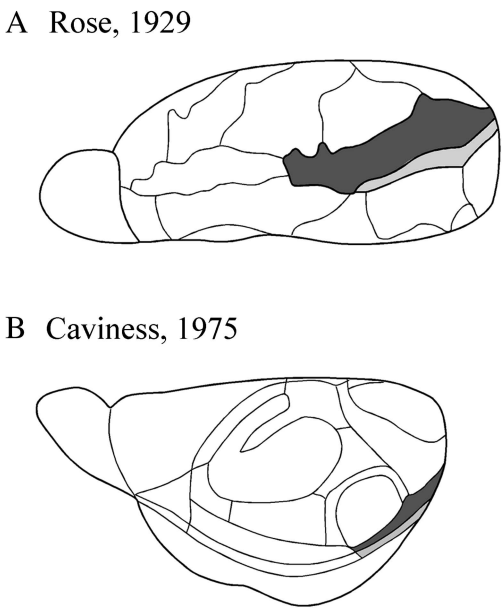

Figure 1. Historical views of the mouse cortical mantle. (*A*) Lateral surface view of the mouse brain adapted from Rose (1929). Ectorhinal cortex is shown in dark gray and perirhinal cortex is shown in light gray. (*B*) Dorsolateral surface view adapted from Caviness (1975). Area 36 is shown in dark gray and area 35 is shown in light gray. Note that the perspectives differ in these 2 views. Both views describe the rostral limit of the perirhinal areas as arising at the caudal limit of the claustrum. The dorsal border is more dorsal in Rose (1929), though this is overemphasized, here, because of differences in perspective. See text for details about nomenclature.

ectorhinalis," whereas Caviness (1975) used the numeric designations, that is, areas 35 and 36. Rose (1929) included area perirhinalis in the retrohippocampal areas along with the entorhinal, presubicular, and parasubicular cortices. He included area ectorhinalis in "Regio occipitalis" along with striate and occipital cortex, noting, however, the extraordinarily weak granule layer as evidence against inclusion in Regio occipitalis. Similarly, Caviness (1975) included area 36 in the temporal region and area 35 in the retrohippocampal region. However, he observed that the cytoarchitecture and myeloarchitecture of area 35 is unlike the other retrohippocampal regions and much more resembles area 36.

The issue of structural similarities between area 35 and area 36 are also evident in the primate homologues. Van Hoesen and Pandya (1975) dropped the term ectorhinal cortex and used the term perirhinal cortex to designate the combined areas 35a and 35b, which are analogous to Brodmann's areas 35 and 36. Amaral et al. (1987) considered the 2 regions sufficiently different to retain Brodmann's terminology of areas 35 and 36 but did apply the term perirhinal cortex to designate the combined areas. This nomenclature is now widely utilized in research on nonhuman primates. Additionally, we have adopted this nomenclature in our neuroanatomical studies of these areas in the rat brain (Burwell and Amaral 1998a, 1998b; Burwell 2001). Thus the term, perirhinal cortex is commonly used, but the term "ectorhinal" is no longer in use for nonhuman primates and rarely used for rodents except in stereotaxic atlases.

The disadvantage of the older terminologies is that they lack correspondence across species and thus hamper the use of mouse models of human parahippocampal function. The recent mouse atlases also regrettably use the older rodent terminology (Hof et al. 2000; Dong 2008; Franklin and Paxinos 2008; Paxinos and Watson 2010). Fortunately, the only available careful review of the anatomy of the mouse hippocampal system does use the terms postrhinal cortex and perirhinal areas 35 and 36 (Witter 2010).

Aside from nomenclature, the other issue to be addressed is disagreement about the borders of the perirhinal area. The border with the ventrally adjacent entorhinal cortex is now well documented (van Groen 2001), and there is substantial agreement. The historical disagreements in the other borders remain at issue. As represented in Figure 1, there are discrepancies in the rostrocaudal location of the border between the perirhinal regions and the insular cortex as well as the dorsal border of area ectorhinalis/area 36. Additionally, neither of the classic studies depicted in Figure 1 defined a region in the mouse brain comparable to the rat POR and the monkey parahippocampal cortex. An examination of modern descriptions of these areas confirms that the location of the rostral and dorsal boundaries of the PER and the presence of POR are open questions for the mouse model (Franklin and Paxinos 1997; Hof et al. 2000; Paxinos and Franklin 2001). In the present study, we have used a comparative approach, relying on what is known in the rat and primate as well as inbred mouse strains, to address these open questions in the mouse brain.

Historically inbred mouse strains have been an invaluable tool for genetics research. Research conducted in that tradition has revealed that inbred mouse strains can differ dramatically in learning and memory capabilities, for example, acquisition of a water version of the radial-arm maze (Hyde et al. 1998), standard water maze performance, and fear conditioning (Owen et al. 1997). Even substrains of inbred mouse strains can show marked genetic variability (Simpson et al. 1997) and differing behavioral phenotypes (Montkowski et al. 1997). Research on memory using mice often employs the C57BL/6 strain, perhaps because of reports that mice from that inbred strain perform better than others on some memory tasks, for example, the water maze (Upchurch and Wehner 1988). C57BL/6 mice, however, begin to lose hearing at about 7 months of age (Willot 1986) and are poor avoidance learners (Schwegler and Lipp 1983).

Although the comparative analysis of inbred mice strains has been fruitful, inbred strains may not provide the best genetic background for modern molecular approaches to understanding brain–behavior relationships. The use of first-generation hybrid (F1) mice eliminates the potential of homozygous alleles to produce abnormal behavioral phenotypes. For example, F1 hybrid mice perform better than inbred strains on tests of hippocampal-dependent memory (Upchurch and Wehner 1988; Owen et al. 1997). Indeed, on the Morris water maze, F1 hybrids perform more similarly on probe trials to one another than to their parent inbred strains (Owen et al. 1997). Indeed, we recently identified attentional deficits in an F1 mouse model of Fragile × Syndrome (Casten et al. 2011). It was necessary to use the F1 model because wild-type mice of the inbred parent strains were unable to learn the task. F1 mice, similar to inbred strains, are advantageous because all mice share an identical genotype.

There is now considerable evidence that using F1 hybrid strains is an advantageous approach to controlling genetic background in the behavioral analysis of mutant and transgenic mice (Wolfer and Lipp 2000; Estill et al. 2001; Voikar et al. 2001; Lipp and Wolfer 2003). The approach has been used to study, for example, drugs of abuse (Walters and Blendy 2001),

signaling pathways in learning and memory (Gass et al. 1998; Graves et al. 2002), and the pharmacology of locomotor behavior (Kelly et al. 1998). The above review highlights the importance of controlling genetic background in the use of transgenic and gene-targeted mice as models to study learning, memory, and plasticity. Indeed, a conference composed of primary investigators using mice in neurobiological research developed a set of recommendations, one which advised use of F1 mice as the genetic background whenever possible (Silva et al. 1997). It was further suggested that the parent strains be the C57BL/6 and the 129/J. We followed that recommendation in the present anatomical study, as well as in our functional studies.

Here, we report cytoarchitectonic and histochemical observations from F1 B6129PF/J1 mice and compare our findings with data collected from the parent inbred strains, the C57BL6/J and 129P3/J, as well as data collected from rats. Clarification of the cytoarchitecture of these regions in the mouse will inform research addressing the neural basis of memory and the function of structures within the medial temporal lobe.

Materials and Methods

Subjects

Subjects were 39 untreated adult male mice weighing between 24 and 48 g (median 32 g). The mice ranged from 16 to 26 weeks of age (median 22 weeks). Thirty subjects were F1 mice (B6129PF/J1). Cases were also prepared from the parent inbred mouse strains, C57BL6/J (n = 4) and 129P3/J (n = 4). All cases were consulted. Based on the quality of the tissue preparations, 19 cases were extensively analyzed with detailed notes, illustrations, and/or photographs. Tissue prepared from 2 F1 mice, one C57BL6/J mouse, and one 129P3/J mouse were photographed for illustration purposes. All subjects were obtained from the Jackson Laboratory (Bar Harbor, Maine). Animals from the same strain were housed together in plastic cages in groups of 3–5 with ad libitum access to food and water. All methods involving the use of live animals conformed to NIH guidelines and were approved by the Brown University Institutional Animal Care and Use Committee.

Tissue Processing

Animals were deeply anesthetized with Beuthanasia-D (0.05 mL/25 g intraperitoneal, Schering Plough Kenilworth, N.J.) and were immediately transcardially perfused with a peristaltic pump at a flow rate of 10–15 mL/min. Perfusion procedures optimized for the Timm's procedure were adapted from Sloviter (1982). Mice were perfused with 0.37% sulphide solution (pH 7.2) for 5 min followed by 10% buffered formalin solution (pH 7.2, 1.23 M formaldehyde in 0.1 M phosphate buffer) for 15 min. Brains were immediately removed from the skull and cryoprotected for 24–48 h in 10% formalin and 20% glycerin in 0.1 M sodium phosphate buffer (pH 7.4) at 4 °C.

Each brain was blocked according to the plane of section (i.e., coronal, sagittal, or horizontal). Brains that were not sectioned immediately were stored at –80 °C until processing. The brains were sectioned in the coronal (n = 37), sagittal (n = 3), horizontal (n = 2) plane at 30 μm using a freezing microtome. The tissue was then processed for visualization of Nissl material, myelinated fibers, heavy metals, and the enzyme acetylcholinesterase (AChE) using procedures similar to those used in earlier studies of the rat brain (Burwell 2001). These preparations were chosen based on consultation of archival material and because they were useful in similar analyses of the corresponding regions in the rat brain (Burwell 2001). For comparison with other species, limited material was also processed for visualization of parvalbumin and nonphosphorylated neurofilament. Sections were collected in 6 series such that a set of neuroanatomical markers could be examined in adjacent sections. One series was collected in 0.1 M sodium acetate buffer (pH 6.0, adjusted with glatial acetic acid) for subsequent staining for the AChE. A second series was collected in 0.1 M phosphate buffer (pH 7.4) for the Timm's procedure. Two series were stored in 10% buffered formalin for subsequent processing using cell and fiber stains. The 2 remaining series were collected in a tissue cryoprotectant solution consisting of 30% ethylene glycol and 25% glycerin in 0.1 M sodium phosphate buffer (pH 7.4) and stored at –20 °C.

Nissl and Fiber Stain

We used standard thionin staining techniques for demonstration of Nissl material. Two series of sections were stored in 10% formalin solution for at least 1 day. For Nissl staining, the tissue was thoroughly rinsed in 0.1 M buffered phosphate and mounted on gelatin-coated slides. The mounted sections were dried in a 36 °C oven for at least 1 day. Slides intended for cell stain were defatted in a solution of one part chloroform and one part 100% ethanol followed by hydration in a descending series of alcohol solutions. The mounted sections were stained in a 0.25% thionin solution and differentiated in dilute glacial acetic acid, 2–6 drops in 250 mL of 95% ethanol. Slides were dehydrated in an ascending series of alcohol solutions followed by immersion in xylene. Sections were then coverslipped using DPX mountant (BDH Laboratory Supplies, Poole, England). For visualization of myelinated fibers, we used a gold chloride staining procedure that uses trace amounts of hydrogen peroxide (Schmued 1990; Quinn and Graybiel 1994; Burwell 2001). Free-floating sections were rinsed in phosphate-buffered saline (PBS) (0.2 M phosphate and 0.10 M sodium chloride at pH 7.4) and incubated in 0.2% gold trichloride trihydrate and 0.012% H_2O_2 in the same 0.2 M PBS for up to 4 h. The reaction was terminated when fibers in the entorhinal cortex were clearly visible. Sections were rinsed in normal saline (0.9% sodium chloride) for 10 min, fixed in a 5% sodium thiosulfate solution for 5 min, and rinsed in 0.2 M PBS (3 × 5 min). Sections were mounted on gelatin-coated slides and dried for at least 1 day in a 36 °C oven. After drying, the tissue was dehydrated in ascending alcohols, immersed in xylene, and coverslipped with DPX mountant (see procedures for cell stain).

Timm's Sulphide Silver Stain

We processed one series of sections for the demonstration of heavy metals according to the Timm's sulphide silver method (Sloviter 1982). Sections collected into 0.1 M phosphate buffered solution (pH 7.4) were mounted on the same day on acid-washed, gelatin-coated slides. Sections were dried for 24 h in a 36 °C oven, defatted in xylene, and hydrated in a descending series of alcohols. The slides were allowed to dry at room temperature for 1–2 h before processing. All solutions were prepared in acid-washed glassware. Aliquots of 33% solution of gum Arabic (Sigma-Aldrich, St Louis, MO) were prepared in distilled water and frozen for the Timm's procedure. On the day of processing, the gum Arabic solution was thawed, and stock solutions of 0.5 M hydroquinone and 2.0 M citrate buffer (pH 7.2) and 20% silver nitrate in distilled water were prepared under normal light conditions. Immediately prior to the beginning of processing, we prepared, under safelight (Kodak filter 1, red) conditions, a solution of 30% 0.5 M hydroquinone, 10% 2.0 M citrate buffer (pH 7.2), and 60% stock gum Arabic in distilled water. To begin the reaction, the equivalent of 0.05% of the 20% silver nitrate solution was added to the solution and gently mixed in darkroom conditions. The slides were submerged for approximately 30–60 min depending on visual assessment of the speed of the reaction. The reaction was stopped when all 3 sublayers of the dentate gyrus molecular layer were visible at 40X. The slides were then washed in running tap water for 10 min in the dark. The remaining steps were carried under normal light conditions. After rinsing 2 × 2 min in distilled water, the sections were fixed for 12 min in 5% sodium thiosulfate in distilled water, dehydrated in an ascending series of alcohol solutions, and finally coverslipped from xylene with DPX mountant.

AChE Stain

We processed one series for the demonstration of the enzyme AChE using a procedure adapted from Hedreen et al. (1985). The procedure was conducted on the day that the brain was sectioned. The enzymatic reaction was carried out upon free-floating sections in 15-mm

polypropylene netted wells and carrier kits (Fisher Chemicals, Fairlawn, NJ). Sections were collected in 0.1 M sodium acetate buffered solution (pH 6.0). A solution was prepared of 65% 0.1 M sodium acetate buffer, 5% 0.1 M sodium citrate buffer (pH 6.0), 10% 0.03 M cupric sulfate, and 4% 0.005 M potassium ferricyanide in distilled water. The equivalent of 0.05% acetylthiocholine iodide and 0.007% ethopropazine (Sigma-Aldrich) were added and dissolved at room temperature to block nonspecific cholinesterases. The sections were incubated in this solution at room temperature for 30 min on a shaker table. Following incubation, sections were rinsed 3 × 5 min in 0.1 M sodium acetate buffer (pH 6.0), incubated in 4% ammonium sulfide for 1 min, rinsed 3 × 5 min in 0.01 M sodium nitrate buffer (pH 7.2), and then intensified in 0.1% silver nitrate in distilled water for 1 min. Following intensification, the tissue was washed 3 × 5 min in the same 0.01 M sodium nitrate buffer and mounted on gelatin-coated slides. The mounted sections were allowed to dry overnight at room temperature. After drying, the sections were dehydrated as described previously through an increasing series of alcohols and coverslipped from xylene with DPX mountant.

Parvalbumin Immunohistochemistry

Immunohistochemical processing for visualization of parvalbumin-immunoreactive cells was accomplished by the following procedure. The sections were washed 3 times in PBS (0.1 M phosphate and 0.15 M NaCl, pH 7.4) and incubated in 0.5% H_2O_2 in PBS for 45 min to quench endogenous peroxidases. The tissue was then washed 3 × 5 min in PBS and placed in 0.25% TX-100 in PBS for 45 min. After rinsing in 0.1% Tween-20 (Sigma-Aldrich) in PBS, and sections were incubated for 1 h in 0.1% Tween-20 and 10% normal horse serum (NHS) in PBS as a blocking step to minimize nonspecific binding. Following blocking, the sections were incubated overnight in the primary antibody (1:10 000 mouse anti-parvalbumin [no. 325, Swant, Bellinzona, Switzerland], 0.25% TX-100, 10% NHS, in PBS). The next day, the sections were rinsed 5 × 5 min in 0.1% Tween-20 in PBS and then incubated for 2 h in the secondary antibody (1:200 biotinylated horse anti-mouse IgG [BA-2001, Vector Laboratories, Burlingame, CA], 0.25% TX-100, 10% NHS, in PBS). After rinsing, 5 × 5 min in 0.1% Tween-20 in PBS, the sections were processed in an avidin–biotin reaction for 2 h, followed by 3 × 5 min rinse in 0.1% Tween-20 in PBS and one 5 min rinse in PBS. The sections were developed in diaminobenzidine tetrahydrochloride (Sigma-Aldrich) and rinsed in PBS to stop the reaction. The sections are mounted, dehydrated in graded ethanols and xylenes, and coverslipped.

Location of Bregma and Lambda

To determine the rostrocaudal location of coronal sections for the F1 mice, we stereotaxically demarcated bregma and lambda in 5 anesthetized mice. Subjects were deeply anesthetized with a 3% isoflurane/oxygen mixture and maintained at 1.5–2% isoflurane. Four injections of 30 nL of 3% Fast Blue (Dr. Illing, GmbH and Co., Gross Umstadt, Germany) in distilled water was stereotaxically injected at 2.0 mm and –2.0 mm lateral to the midline at Bregma and lambda. All 4 sites were 3.0 mm ventral to skull. The animals were immediately perfused and the brains were prepared and sectioned coronally, as described above, with the following exceptions: the animals were initially perfused with 0.9% saline, followed by 10% formalin, and the brain was sectioned at 40 μm and collected in a 1:5 series. Shrinkage was calculated by dividing the rostrocaudal distance between lambda and bregma by the number of sections between lambda and bregma, such that coronal levels relative to bregma could be determined. These designations were used for illustrations and in the text, unless noted otherwise.

Analysis and Photomicroscopy

Histochemical and cell-stained preparations for all cases were systematically examined at several magnifications. Serial sections were examined microscopically, and some cases were photographed for ease of analysis. Documented characteristics included cell morphology, myeloarchitecture, and laminar and regional staining patterns. Serial sections for several representative cases were photographed, and one was selected for illustration of the cytoarchitectonic, histochemical, and myeloarchitectonic organization of the PER and POR. The regions analyzed are shown on a schematic of the lateral surface of the mouse brain and in an unfolded map (Fig. 2). Digital photomicrographs were acquired with an SPOT RT digital camera (Diagnostic Instrument, Sterling Heights, MI) and composites assembled with Adobe Photoshop 5.5. Text, laminar outlines, and borders were added using Canvas 7.0 (Deneba Software, Miami, FL).

Nomenclature

In the present report, we use Brodmann's (1909) numeric nomenclature for areas 35 and 36, but we have designated the combination as perirhinal cortex and have dropped the term, ectorhinal cortex. This terminology was chosen to be consistent with our terminology in the rat (Burwell 2001) and terminology in the monkey (e.g., Suzuki and Amaral 2003). Terminology for the caudal region, that is, the POR, is also consistent with our earlier work in the rat (Burwell et al. 1995; Burwell 2001).

Borders for the entorhinal cortex were taken from van Groen (2001) and are consistent with the division proposed by Rose (1929) for the mouse entorhinal cortex (Fig. 1*A*) and by Insausti et al. (1997) for the rat entorhinal cortex. Other borders were taken as needed from Hof et al. (2000) or Paxinos and Franklin (2001). Unless otherwise noted, terminology was taken from Hof et al. (2000).

Results

The following description includes cytoarchitectonic, myeloarchitectonic, and histochemical characteristics of PER areas 35 and 36 and the POR of the F1 mouse brain. In general, we focused on the cytoarchitectonic and histochemical features that most reliably characterize the ROIs and on those features that differentiate subfields of a region. For demonstration purposes, photomicrographs of a representative case of coronal

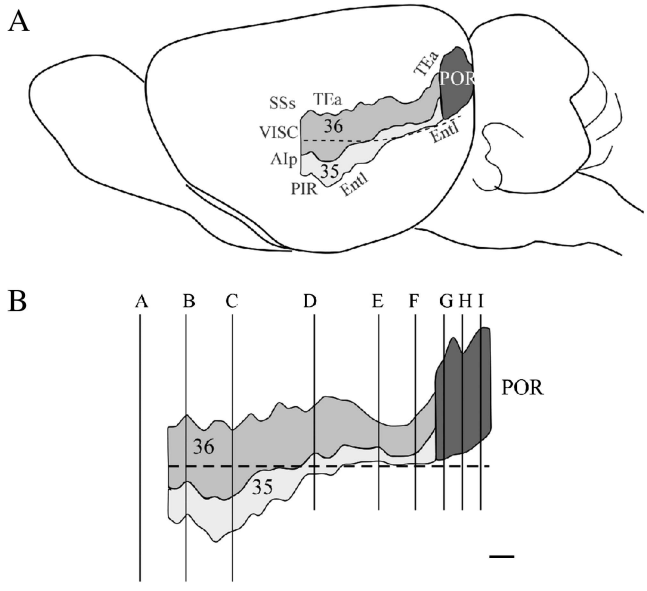

Figure 2. Perirhinal (PER) and postrhinal (POR) cortices of the mouse. (*A*) Lateral surface view of the mouse brain illustrating the borders. (*B*) Unfolded map of the perirhinal and postrhinal cortices of a representative case. In both *A* and *B*, the dashed line indicates the rhinal fissure. Coronal levels illustrated in Figures 3, 4, 7, and 10 are indicated by vertical lines. Letters associated with each level correspond to the panels in Figure 3. Scale bar (panel *B*) = 250 μm. Other abbreviations: 36, area 36; 35, area 35; AIp, posterior insular cortex; Entl, lateral entorhinal area; PIR, piriform cortex; PORd, dorsal POR; PORv, ventral POR; TEa, temporal association areas; VISC, visceral area.

sections were taken at 9 rostrocaudal levels (Fig. 3). Each case included series stained for Nissl, heavy metal by the Timm's method, AChE, and myelin. Two additional hybrid mouse cases also included parvalbumin. The parvalbumin was found to be redundant with the Timm's stain for identifying borders, and no additional cases were prepared. This material will be only briefly described in the Results. The Timm's stain proved to be most useful in identifying regional borders as it exhibits staining patterns highly comparable to those observed in the rat (Burwell 2001). The AChE and myelin were less useful, therefore one or the other, but not both, is included in photomicrographs or coronal sections at each of the 9 levels. It should be noted that we frequently used the rhinal fissure as a general landmark. Though not as reliable as in the rat brain, the fundus and both banks are visible on the lateral surface of the F1 mouse brain. This feature may not be as prominent in inbred parent strains (Hof et al. 2000).

Perirhinal Cortex

The PER comprises 2 narrow, horizontal bands of cortex, areas 35 and 36, positioned such that area 36 lies dorsal to area 35 (Fig. 2). The PER is bordered rostrally by insular cortex and caudally by the POR. For most of its rostrocaudal extent, the PER shares its ventral border with the dorsolateral field of the lateral entorhinal cortex (ENTl). At the rostral limit, the PER is bordered dorsally by secondary somatosensory cortex (SSs). At midrostrocaudal levels, secondary auditory cortex (AUDv) is located dorsal to the region; caudally, ventral temporal association cortex (TEA) is dorsally adjacent. Figure 3 shows coronal sections for 9 rostrocaudal levels including 5 levels of the PER. Photomicrographs of those 5 coronal levels are shown in Figures 4 and 5.

In the mouse brain, the association of areas 35 and 36 with the rhinal fissure changes as one moves from rostral to caudal levels. At rostral levels in most animals, area 36 includes the

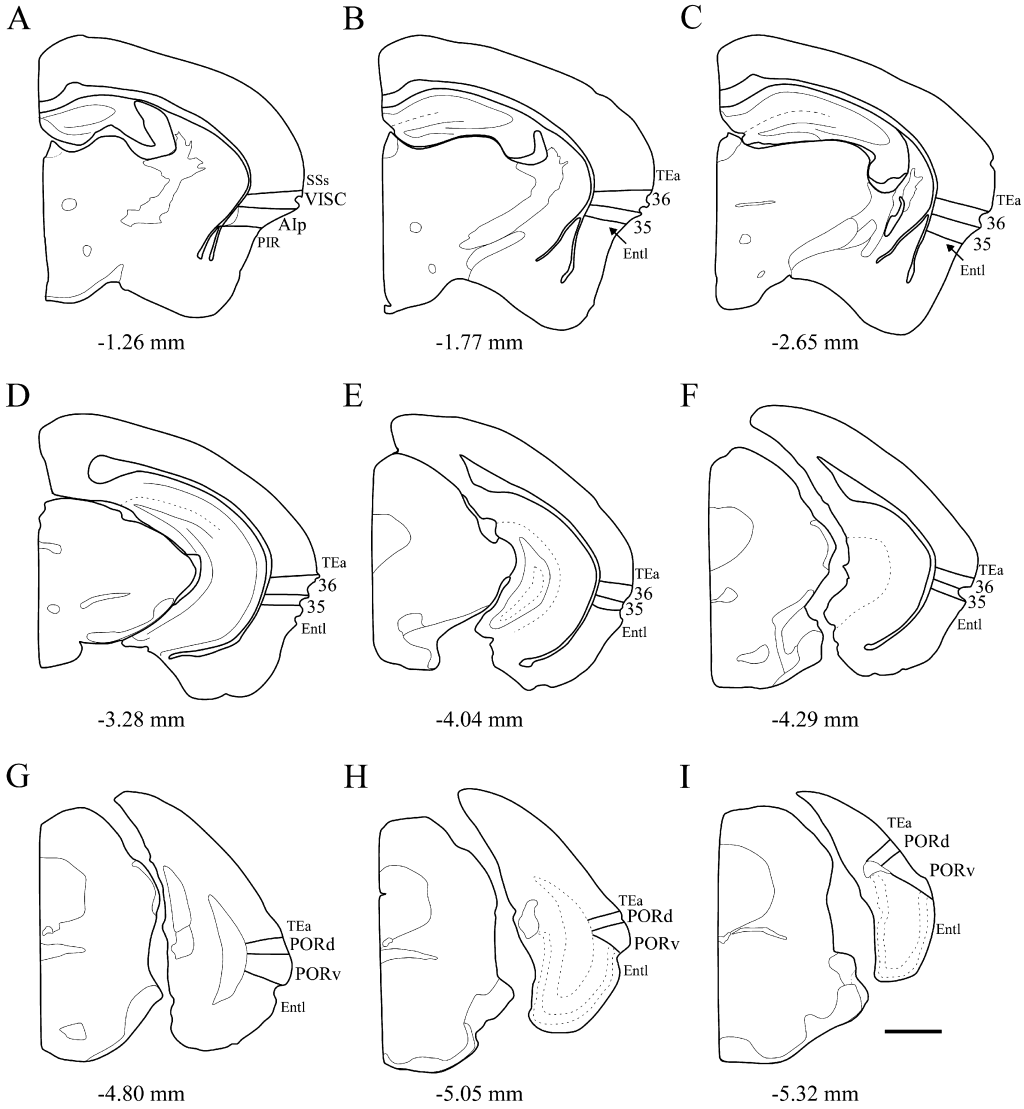

Figure 3. Schematic of the mouse brain showing 9 rostrocaudal levels in the coronal plane. Levels on the top row, middle, and bottom rows are those shown in Figures 4, 5, and 10, respectively. Rostral to caudal levels are identified relative to bregma coordinates for a representative male first-generation hybrid, B6129PF/J1, weighing approximately 30 g at about 12 weeks of age. Scale bar = 1000 μm. Abbreviations: 36, area 36; 35, area 35; AIp, posterior insular cortex; Entl, lateral entorhinal area; PIR, piriform cortex; PORd, dorsal POR; PORv, ventral POR; TEa, temporal association areas; VISC, visceral area.

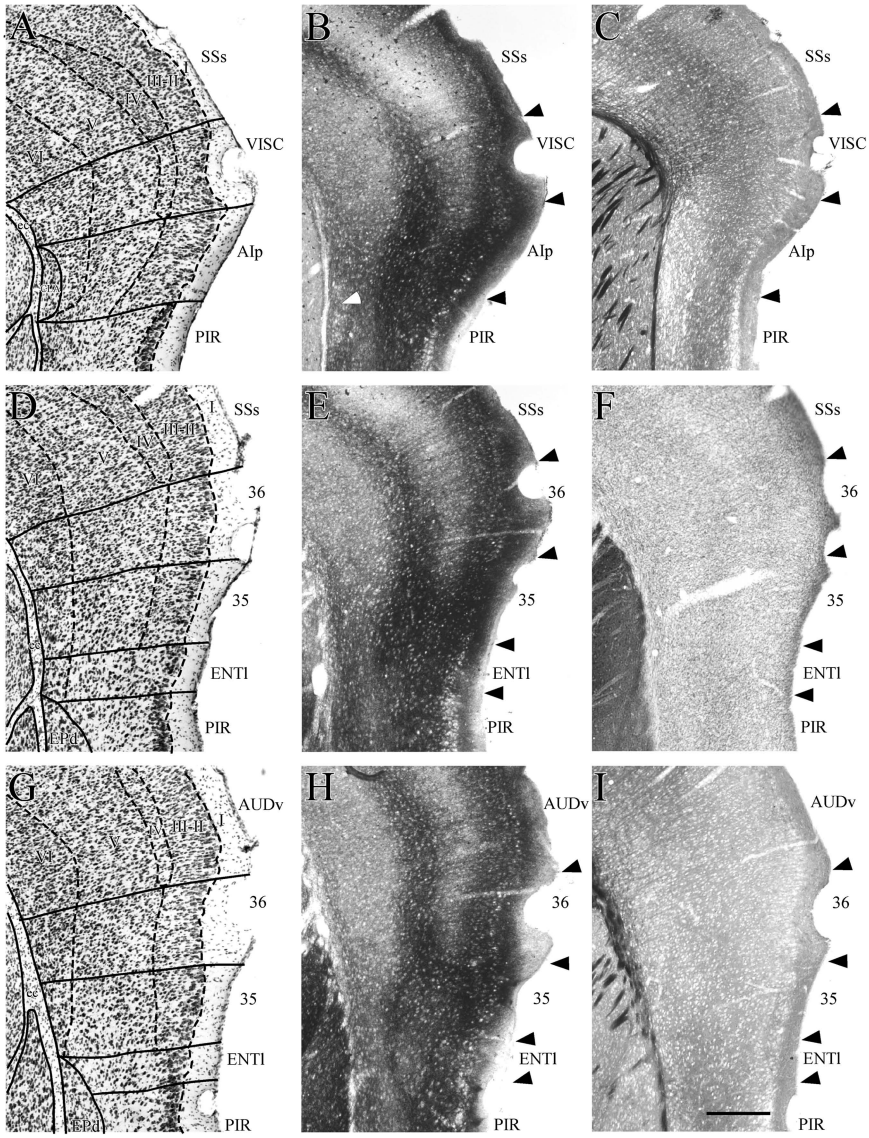

Figure 4. Coronal sections showing rostral perirhinal cortex (PER) and bordering regions. Shown are the rostrally adjacent insular region (VISC) at one level (top row) and the perirhinal areas 35 and 36 at 2 rostrocaudal levels (middle and bottom rows). At each level, adjacent sections were stained for Nissl material (*A*,*D*, and *G*), heavy metals using Timm's method (*B*, *E*, and *H*), myelinated fibers (*C* and *I*), and the enzyme acetycholinesterase (*F*). The claustrum, located deep to insular cortex, is easy to identify in Nissl and Timm's material. It is outlined in panel *A* and designated by the white arrow in panel *B*. Other abbreviations: AIp, posterior agranular insular; AUDv, ventral auditory cortex; ec, external capsule; ENTl, lateral entorhinal area; EPd, the dorsal part of endopiriform nucleus; PIR, piriform cortex; SSs, secondary somatosensory.

fundus and both banks of the rhinal fissure, and area 35 occupies the location ventral to the fissure (Fig. 3, panels *B* and *C*). Proceeding caudally, areas 35 and 36 rise until they lie above the fundus of the rhinal fissure. At the caudal end of the PER, the ventrally adjacent entorhinal cortex includes the ventral bank of the rhinal fissure. In the case illustrated here, the association of the PER with the rhinal fissure is better discerned at midrostrocaudal levels, where the rhinal fissure is more deeply invaginated (Fig. 3, panels *F* and *G*). It should be noted that the shape and location of the rhinal fissure in the mouse brain varies across individuals and can be difficult to discern, especially at rostral levels.

Rostral Border with Insular Cortex

Agranular and granular insular cortex are rostrally adjacent to the PER (Fig. 3*A*). These regions correspond to the posterior part of the agranular insular area (AIp) and the visceral cortex (VISC) according to Hof et al. (2000) or to AIp and granular and dysgranular insular cortices (GI/DI) according to Franklin and Paxinos (2008). In coronal sections of cell-stained material, the insular cortex can be readily identified as the cortex that overlies the claustrum, a mass of darkly stained and densely packed cells positioned deep to insular layer VI (Fig. 4*A*–*C*). In Timm's material, the claustrum stains less darkly for heavy metals than the overlying insular cortex does (Fig. 4*B*, white arrow). Proceeding caudally, the claustrum shrinks and flattens into a progressively smaller nucleus of darkly stained, disorganized medium-sized elongated cells that are roughly parallel to the surface of the external capsule. When the claustrum is no longer present, insular cortex is replaced by the PER.

The insular region can be identified by its tri-laminate appearance at low magnification (not shown). The transition from

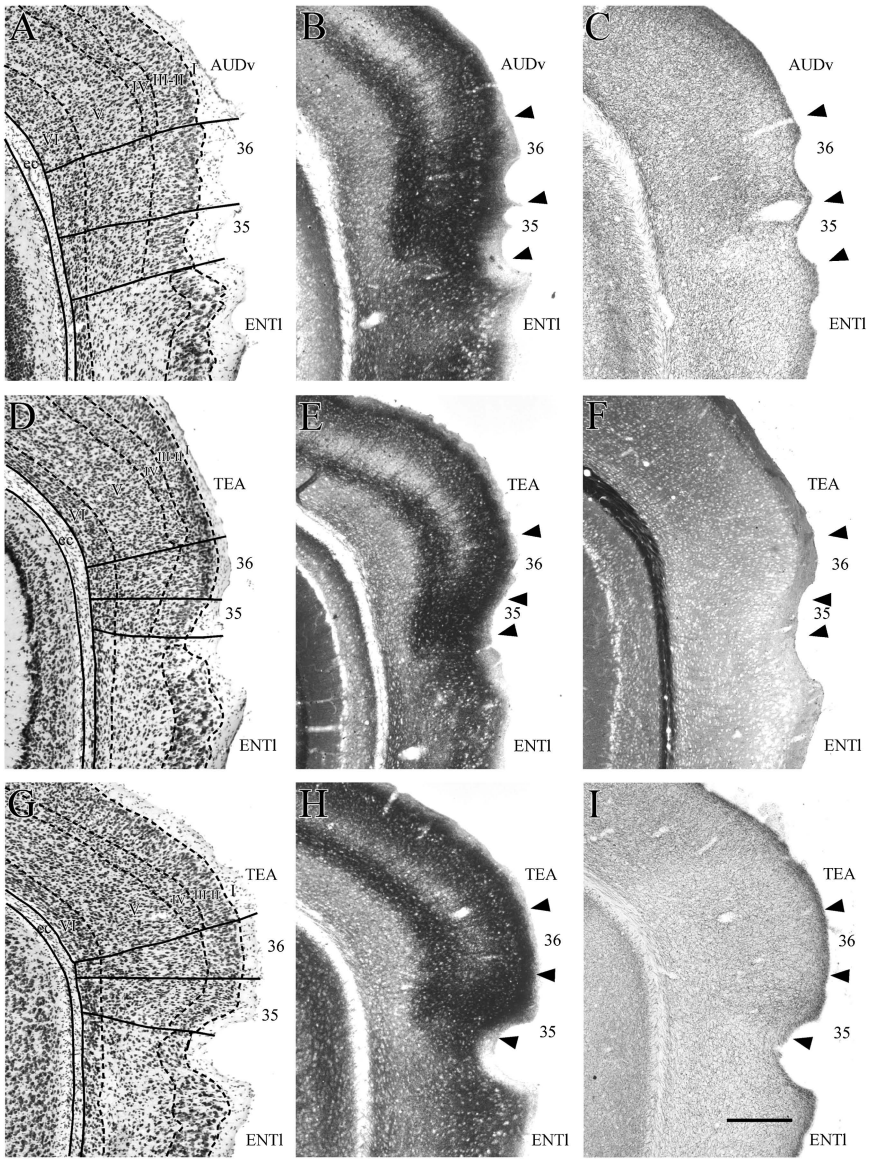

Figure 5. Coronal sections showing caudal perirhinal (PER) areas 35 and 36 and adjacent cortical regions at 3 rostrocaudal levels. Adjacent sections stained for Nissl material (*A*, *D*, and *G*), heavy metals using Timm's method (*B*, *E*, and *G*), myelinated fibers (*F*), and the enzyme acetycholinesterase (*C* and *I*). Other abbreviations: AUDv, ventral auditory cortex; ENTl, lateral entorhinal area; PIR, piriform cortex; SSs, secondary somatosensory; TEA, temporal association area.

insular regions to PER is characterized by a more homogeneous look in the PER (Figs 4*D* and 6) as compared with the trilaminar look of the insular regions (Fig. 4*A*). This is because layer V is broader and somewhat more densely populated in the PER.

In insular regions, superficial layers II–III/IV and layer VI contain more darkly staining and densely packed cells than those of the intervening and more sparsely populated layer V. Other features are better observed at higher magnification (Fig. 7, panels *A* and *B*). Layer II contains medium-sized round and oval cells that merge into the small and medium pyramidal cells of layer III. Layer II cells tend to be smaller in VISC (Fig. 7*A*) than in AIp (Fig. 7*B*). A narrow layer IV of granule cells is apparent in VISC, but AIp does not have a discernable layer IV. Layer V contains medium-sized dark pyramids, and layer VI contains round and polygonal, medium to small, darkly staining cells.

Area 36 Borders and Cytoarchitecture

Area 36 is bordered rostrally by VISC, dorsally by the secondary SSs at rostral levels, by the ventral and posterior auditory association cortex (AUDv and AUDp) at midrostrocaudal levels, and by the temporal association area (TEA) at the most caudal levels. Ventrally, area 36 is bordered by area 35 and caudally by the POR.

At rostral levels, area 36 is associated with the rhinal fissure (Figs 3*B*,*C* and 4*D*–*I*). Except for layer II, the packing density is relatively similar across all layers. Layer II has a somewhat patchy look (Fig. 8*B*). The cells are large, round, and tending to be lightly stained. The dorsally adjacent SSs has smaller cells in layer II (Fig. 8*A*). Layer III contains small pyramids. Layers II and III are more easily distinguished in 36 than SSs. At rostral levels, layer IV is difficult to discern, although some granule cells are mixed in at the border between layers III and V. This is evident

in the horizontal plane (Fig. 6*A*, left or rostral side of panel). Superficial layer V has small pyramids that are progressively larger and more darkly staining moving from the superficial to deep part of the layer. Cells are more sparsely packed in V especially superficially. Layer VI contains a variety of disorganized medium-size polymorphous cells that stain darkly. In some cases, the deepest layers are flattened parallel to the external capsule.

At midrostrocaudal levels (Figs 3*D* and 5*A*–*C*), area 36, which is located above the rhinal fissure, has a smaller cortical depth (Figs 3*D* and 5*A*–*C*). Most features of the region are similar to more rostral levels of the region with a few exceptions: cells in layer III tend to be organized in lines perpendicular to the pial surface, layer V is more homogeneous, and the varied-shaped cells in layer VI are smaller and more darkly staining (Fig. 8*C*). The dorsally adjacent AUDv is distinguished by smaller and more densely packed layer II cells. AUDv has a discernable layer IV, and the layer IV in area 36 is becoming more evident (Fig. 6*A*).

At caudal levels (Figs 3*E*,*F* and 5*D*–*I*), area 36 exhibits characteristics that are similar to more rostral levels with a couple of noticeable differences (Figs 3*E*,*F* and 5*D*–*I*). First, the cells in all layers at this level are slightly smaller, darker, and more densely packed. There are still granule cells mixed in between layers III and V. The dysgranular layer IV is most evident at caudal levels. This is best appreciated in the horizontal plane (Fig. 6*A*). Even at this level, however, the cortex is still best described as dysgranular (Fig. 8*D*). The pyramids in layer V show the typical size gradient. Layer VI is more densely packed than Layer V. TEA is located dorsally and is distinguished by a discernable layer IV and a broad layer V.

Area 36 Histochemistry

Other markers also differentiate area 36 from its dorsal cortical neighbors. In sections stained for heavy metals with the Timm's method (Figs 4 and 6, middle panels), area 36 exhibits a pattern of staining that resembles the alternating pattern of light and dark observed in sensory cortex. Layers I, II, and III stain darkly, though superficial layer I is slightly lighter. The dysgranular layer IV stains lightly, and this is most evidence in the horizontal plane (Fig. 6*C*). Layer VI stains lightly but not as lightly as layer IV. Layer V exhibits a trilaminar pattern with a dark internal sublayer bordered on either side by lighter bands. At rostral and midrostrocaudal levels, area 36 can be

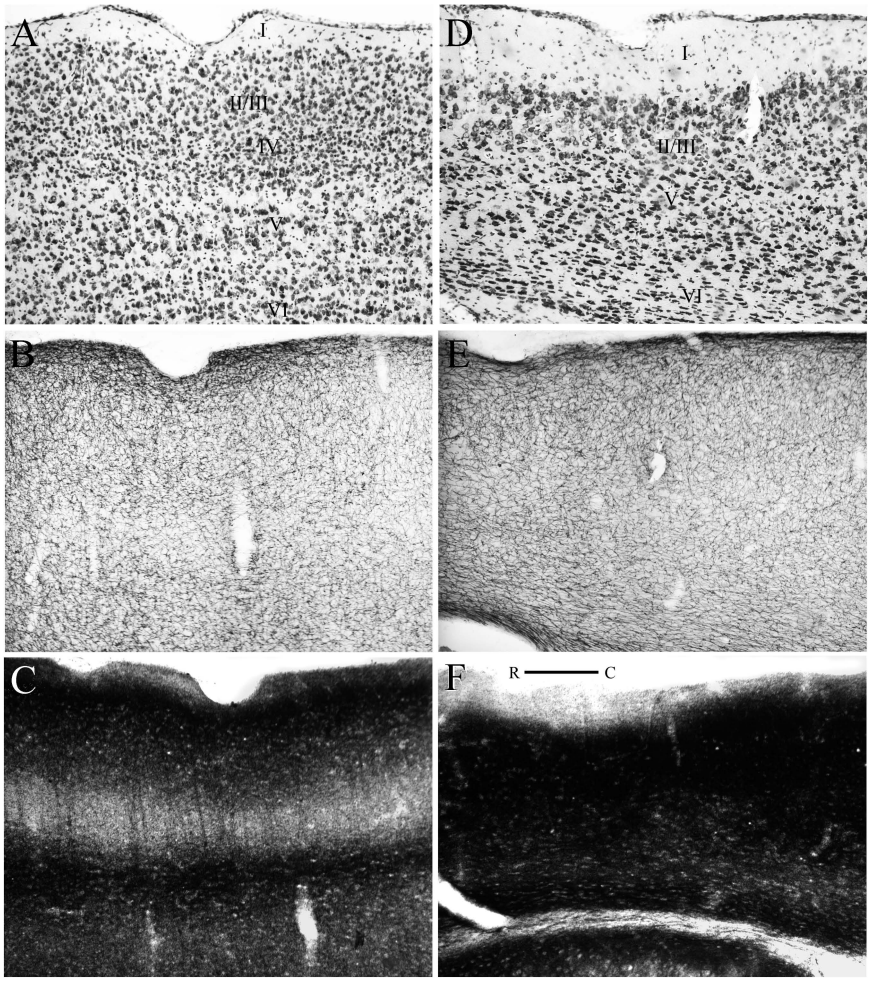

Figure 6. Horizontal sections showing the cytoarchitecture and histochemistry of perirhinal areas 36 (left panels) and 35 (right panels). Adjacent sections were stained for Nissl material (*A* and *D*), the enzyme acetycholinesterase (*B* and *E*), and heavy metals using the Timm's method (*C* and *F*). Note the vestigial granular layer in area 36, panel *A*. Abbreviations: R, rostral; C, caudal. Scale bar = 200 μm.

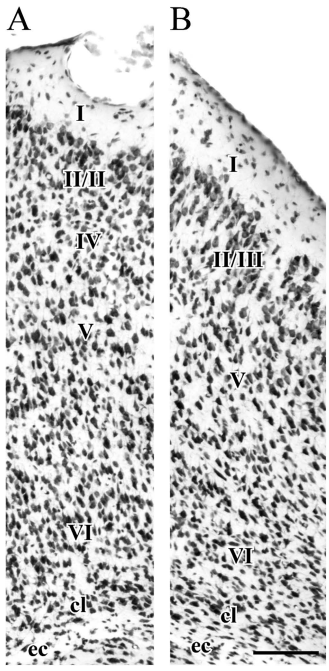

Figure 7. Photomicrographs showing the cortical layers of the insular cortex at –1.20 mm relative to bregma. Sections were stained for Nissl material. VISC has a discrete layer IV (*A*), whereas layer IV of AIp is better described as dysgranular (*B*). Layer V of both VISC and AIp exhibits cells of similar size, staining characteristics, and packing density. Abbreviations: cl, claustrum; ec, external capsule. Scale bar = 100 μm.

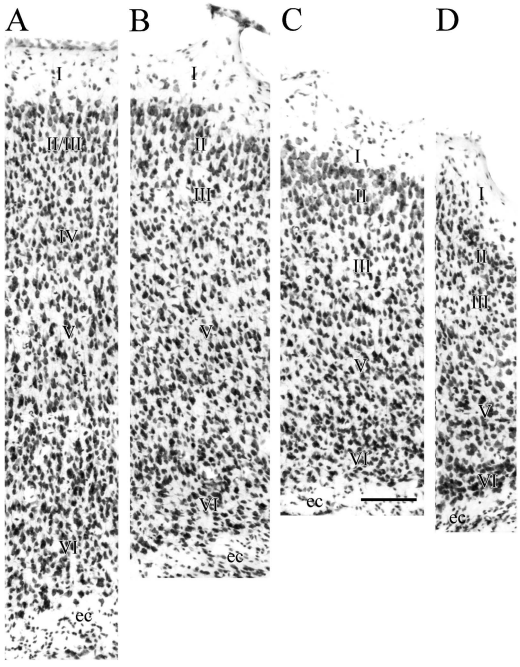

Figure 8. Photomicrographs showing the cortical layers of area SSs (*A*), and area 36 (*B*,*D*) at 3 rostrocaudal levels: –1.77, –2.65, and –4.04 mm relative to Bregma. Sections were stained for Nissl material. Abbreviation: ec, external capsule. Scale bar = 100 μm.

distinguished from the dorsally adjacent SSs and AUDv by the superficial band of layer V that is broader and lighter in the sensory regions (Figs 4*E*,*H* and 6*B*).

The PER exhibits less staining for parvalbumin than the adjacent cortices (not shown). Overall, the pattern of parvalbumin labeling is similar for areas 35 and 36. Another general observation is that parvalbumin labeling decreases from rostral to caudal levels of the region. Rostrally, layers II–III exhibit dense fiber labeling. A few large neurons are labeled in superficial layers. Fiber labeling is lighter in the deeper layers. A few small round cells were observed in layer V. At more caudal levels, more labeled cells were observed in layer V than in layers II–III.

In general, the PER is characterized by the absence of heavily myelinated fibers. Although all but absent in the perirhinal cortex, the bordering regions do contain myelin, thus the stain is useful for visualizing dorsal and ventral perirhinal borders but not for discriminating area 35 from area 36 (Fig. 4*I*).

Area 36 is abundantly labeled with very thin, AChE-positive varicose fibers that form a dense mesh (Figs 4*F* and 6*E*). Occasional neurons are also lightly stained. The density of fiber labeling is constant with the exception of higher density of fibers in the outer molecular layer. This pattern is different from the dorsally adjacent regions, which exhibit a slightly heavier mesh throughout layers I–IV.

Area 35 Borders and Cytoarchitecture

Area 35 is bordered dorsally by area 36, ventrally by the entorhinal cortex, and caudally by the POR (Figs 3*B*,*C* and 4*D*–*I*). At rostral levels, area 35 lies below the rhinal fissure. Proceeding caudally, the area rises to encompass the fissure. The cortical depth (measured from pia to white matter) of area 35 tends to be narrower than that of the dorsally adjacent area 36, especially at more caudal levels.

Area 35 has an even less laminar appearance than area 36. It can be described as agranular cortex, lacking a granule cell layer entirely. At low magnification, layers II and VI appear only slightly darker than the intermediate layers (Fig. 4*D*,*G*). At rostral levels, the cells in the superficial layers of area 35 stain more darkly than those of area 36. At caudal levels, however, the pattern is reversed (Fig. 7*D*,*G*). In general, layer II of area 35 is more disorganized than layer II of 36 in that its cells do not tend to form lines. At rostral levels, the large pyramids in layer V are of a more uniform size (Fig. 9*A*). At more caudal levels, layer V exhibits the characteristic size gradient in which superficial cells are smaller than cells located in deep layer V (Fig. 9*B*). The large pyramids in deep layer V are heart shaped as has been noted in the rat. Layer VI is narrower than in the above area 36. It contains small dark oval cells flattened against the external capsule and tends to be separated from layer V by a cell-sparse area. Area 35 is easily distinguished from the ventrally adjacent entorhinal cortex, which exhibits a prominent layer II and narrow layer VI.

Area 35 Histochemistry

Area 35 shows a characteristic pattern of staining in coronal sections processed for heavy metals using the Timm's method. All but the most superficial portion of layer I and layer VI stain very darkly (Figs 4*E*,*H* and 7, middle panels). These preparations reveal that layer VI is narrower in area 35 than in area 36. Timm's stain also provides a good border with the ventrally adjacent entorhinal cortex in which superficial layers stain more lightly. The difference is especially noticeable between layer V of area 35 and layer V of the entorhinal cortex. Parvalbumin labeling was similar to that of area 36.

Like area 36, area 35 is devoid of heavily myelinated fibers (Fig. 4*I*). More caudally, this is in contrast to the ventrally

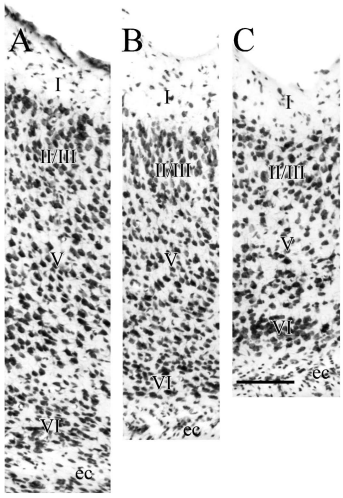

Figure 9. Photomicrographs showing the cortical layers of area 35 at 3 rostrocaudal levels (*A–C*) corresponding to −1.77, −2.65, and −4.04 mm relative to Bregma. Sections were stained for Nissl material. Abbreviation: ec, external capsule. Scale bar = 100 μm.

adjacent entorhinal cortex, which exhibits myelinated fibers in all but layers I and II and the dorsally adjacent temporal association area that contains a plexus of myelinated fibers in deep layers. Thus, although myelination does not distinguish area 35 from area 36, it is a useful marker for determining the borders between the PER and the dorsally and ventrally adjacent cortices.

The pattern of staining for AChE in area 35 is similar to that of area 36 in that the region is filled with a mesh of very thin AChE-positive varicose fibers marked by the occasional lightly stained soma. As with area 36, there is a slightly higher density of fibers in the outer molecular layer (Figs 4*F*, 5*B*, and 8*C,I*).

Postrhinal Cortex

The POR is located caudal to the PER, ventral to TEA, and dorsal to the medial entorhinal cortex (Fig. 2). The POR appears at the caudal end of the angular bundle where subicular cells are no longer visible in coronal sections (Figs 3*G* and 10*A–C*). The POR lies obliquely about the caudal pole, the cells lying deep to the dorsal bank are associated with the entorhinal cortex and not the POR (Fig. 10*A,D,G*). At rostral levels, where the rhinal fissure is still apparent, the POR is above the fundus incorporating a portion of the dorsal bank.

Postrhinal Borders

The POR is bordered rostrally by TEA, however, the boundary is difficult to discern. At the caudal pole, the POR is bordered, ventrally and medially, by the parasubiculum (Fig. 10*G*). In the sagittal plane, the border with the parasubiculum is easily discerned (Fig. 11). The POR lies above the rhinal fissure, although the rhinal fissure in the mouse brain is especially difficult to discern at caudal levels. There is a slight indentation encompassed by the entorhinal cortex at the rostral levels of the POR (Fig. 3*G,H*) but that feature also disappears at more caudal levels (Fig. 3*I*).

The POR is bordered dorsally by the TEA, which can be differentiated by its more discrete layers II and III, layer IV, and the bilaminate look of layer V (Fig. 12*A,B*). Additionally, layer II of TEA differs in that it has smaller cells that are elongated perpendicular to the pial surface. The medial entorhinal cortex borders the region ventrally. The entorhinal cortex differs from the POR in several ways including a distinctive layer II, a clear separation between layers II and III, and a lower packing density in layers III and V (Fig. 12*E*). At caudal levels, the dorsal portion of the POR is bordered medially and ventrally by the parasubiculum (Figs 3*I* and 10*G–I*). At this level in the coronal plane, the POR is triangular in shape. The parasubiculum and the entorhinal cortex form one side of the triangle, TEA forms the second side, and the cortical surface forms the remaining side.

Postrhinal Cytoarchitecture

Cytoarchitectonically, the POR is characterized by a homogeneous appearance and a subtle laminar structure (Fig. 10, panels *A–I*). In the mouse brain, the region can be divided into 2 fields, that is, a dorsal (PORd) and a ventral (PORv) field. The primary cytoarchitectonic difference between the PORd and PORv is the presence of a layer IV in the dorsal subdivision. In this way, PORd is more similar to perirhinal area 36 and PORv is more similar to perirhinal area 35.

The POR can be distinguished from TEA (Fig. 12*A*) by the less differentiated laminar structure. Layer II of PORd has small round cells that stain moderately darkly (Figs 11*D* and 12*B*). The clumpy appearance of POR layer II contrasts with the smooth layer II of TEA and is reminiscent of the patchiness observed in some portions of the PER. Layer III has small round cells similar to those found in layer II, but there are small pyramids mixed in and the layer is less densely packed than layer II. Layer IV contains typical granule cells and is relatively broad, but the borders with deep and superficial layers are not discrete, especially at caudal levels. Thus, the cortex is best described as dysgranular. A broad layer V contains pyramids that show a rough size gradient such that cells tend to be smaller superficially and larger deeper in the layer. Layer VI contains medium-sized, moderately dark-staining round cells that are more densely packed than in layer V.

In the coronal plane, PORv is most easily identified at the rostral limit where layer I is broad and contains ectopic layer II cells near the border with the entorhinal cortex (Figs 10*C* and 11*E*). In the sagittal plane, the POR can be identified by its location dorsal to the parasubiculum (Fig. 11). Rostrally, the layer II cells are slightly larger and lighter than in PORd. There is a tendency for the cells to be slightly elongated giving an oval appearance as opposed to the rounder cells in PORd. The cells in layer III of PORv also have an oval shape. At rostral levels, the oval layer III cells are radially oriented, but this is not the case as one proceeds caudally (Figs 11*E* and 12*C*). Compared with PORd, the cells in layer III are smaller, though just as lightly stained. At rostral levels, layer V has medium pyramids that increase in size as they are located more deeply. The size gradient is more prominent than in PORd. Layer V is more sparsely packed than layer III or VI. Layer VI has small, dark, round cells that are closely packed. At the most caudal level, the region takes on a different look due to the oblique orientation of the cortex around the caudal pole. The coronal plane does not cut perpendicularly across all layers. Thus, PORv has a broad layer II–III. The ectopic II cells are still apparent in some, but not all cases. Layer V is thinner and VI may not be apparent at all.

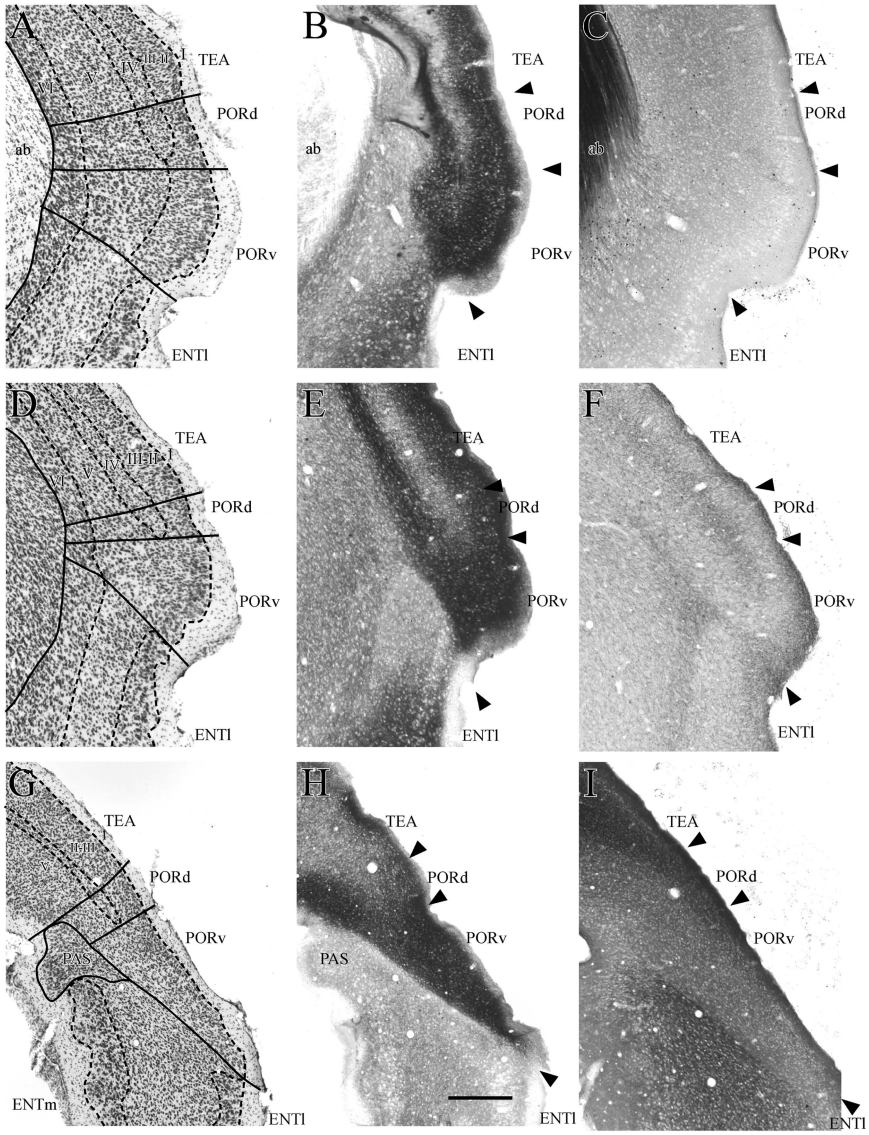

Figure 10. Coronal sections showing the dorsal (PORd) and ventral (PORv) postrhinal cortex and adjacent cortical areas at 3 rostrocaudal levels. Adjacent sections were stained for Nissl material (*A*, *D*, and *G*), heavy metals using Timm's method (*B*, *E*, and *H*), myelinated fibers (*C* and *I*), and the enzyme acetycholinesterase (*F*). Other abbreviations: ab, angular bundle; ENTl, lateral entorhinal area; ENTm, medial entorhinal area; TEA, temporal association area.

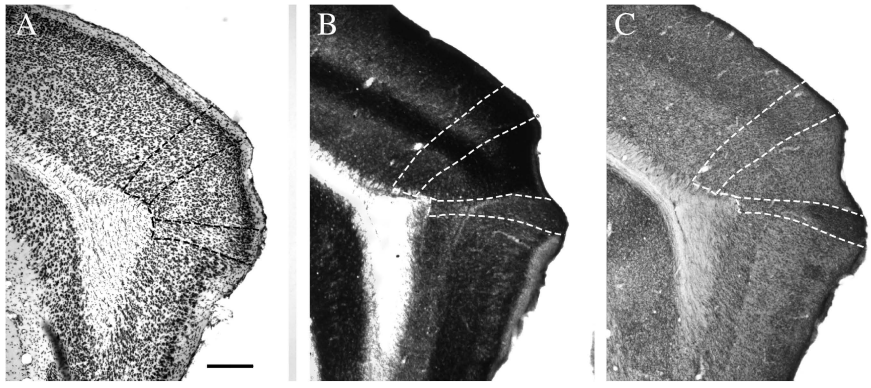

Figure 11. Sagittal sections showing the dorsal (PORd) and ventral (PORv) postrhinal cortex and adjacent cortical areas. Adjacent sections were stained for Nissl material (*A*), the enzyme acetycholinesterase (*B*), and heavy metals using Timm's method (*C*). Scale bar = 200 μm.

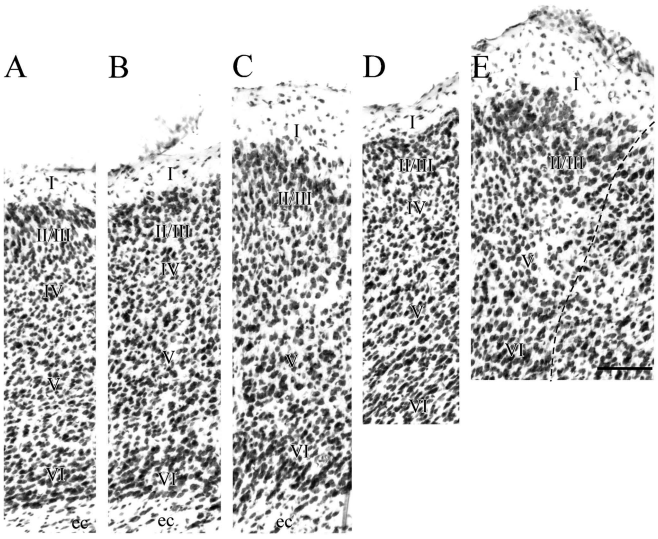

Figure 12. Photomicrographs of the cortical layers of areas TEA (*A*), PORd (*B*), and PORv (*C*) at −4.80 mm relative to Bregma, and PORd (*D*) and PORv (*E*) at −5.05 mm relative to Bregma. Sections were stained for Nissl material. Scale bar = 100 μm.

Postrhinal Histochemistry

In tissue stained for heavy metals using the Timm's method, the PORd shows a laminar pattern such that superficial layer I is light brown and inner layer I is dark brown (Fig. 10*B*,*E*,*H*). Layers II–III are also brown, but layer IV appears as a light band. The superficial half of layer V stains darkly, but the deeper half of layer V and layer VI stain a light reddish brown. PORv exhibits a similar laminar pattern with the exception that it lacks the light layer IV band observed in PORd. Thus, deep layer I through superficial layer V is dark. At the most caudal levels, due to the altered plane of section, PORd has a broad lightly stained layer IV and PORv is entirely dark except for superficial I. At all rostrocaudal levels, the Timm's preparation provides a distinct border with the ventrally adjacent entorhinal cortex. The POR sections stained for parvalbumin exhibit very little labeling and scant cells. Fiber labeling was slightly heavier in PORd than in PORv (data not shown).

Like the PER, the POR exhibits very little myelin. PORd has a few thin myelinated fibers in layers V and VI (Fig. 10*C*). Fibers are thicker and more prominent in TEA. PORv has almost no myelinated fibers. In the entorhinal cortex, myelinated fibers are much more apparent.

As in the PER, the POR exhibits a dense plexus of fibers that stain positively for AChE (Fig. 10*I*). In PORd, the densest label is in superficial layer I. Fibers are less dense in the remaining layers with the exception that layer IV appears slightly darker at low magnification (Fig. 11*C*). The pattern is similar in PORv with the exception that there is no darkening associated with the missing layer IV. The parasubiculum stains very darkly for AChE providing a ventromedial border at caudal levels. At the very most caudal level where the coronal plane does not cut perpendicularly across all layers, the PORd tends to have a broad layer IV and the PORv tends to have broad layers I and II giving the entire region a dark appearance in material stained for AChE (Fig. 10*I*).

Comparison with the Inbred Mouse Strains

The primary analysis was conducted in mice from an F1 line bred from the inbred mouse strains, C57BL6/J and 129P3/J. In this section, we report the results of comparisons between the F1 line and the inbred strains. In both inbred strains, coronal sections stained for heavy metals using the Timm's method yielded staining patterns that were similar to that of the F1 mouse. Thus, the Timm's preparations provided a means for the identification of borders in the inbred strains, which permitted cross-strain comparisons of cytoarchitectonic and other histochemical features.

As in the F1 mouse, the claustrum stains less darkly for heavy metals than the overlying insular cortex in both parent strains. In the F1 mouse, the rhinal fissure is encompassed by VISC. In the C57BL6/J mouse and the 129P3/J mouse, the fissure tends to be more ventrally placed such that it is encompassed by AIp. Also, in both strains, the insular regions have the open, trilaminate look observed in the F1 mouse.

The transition from insular regions to the PER in all 3 strains is characterized by the absence of the underlying claustrum. Additionally, the PER has a more homogenous packing density than the insular region in all 3 strains, but this feature is less evident in the inbred strains as compared with the F1. Similar to the F1, there are 2 sulci associated with the rostral PER in the 2 inbred strains, but the placement in the inbred strains is even more varied across animals and hemispheres. In some 129P3/J cases, packing density is higher, possibly because the overall cortical depth in the 129P3/J is narrower as compared with the F1. Similarly, in some C57BL6/J cases, the packing density is lower, though the cortical depth is similar to the F1.

Some features of area 36 are similar across strains (Fig. 13, left panels). For example, layer II cells tend to be large, light and round, merging into small pyramids of layer III. Layer II is patchy. Layer VI is more densely packed and tends to contain elongated cells that are parallel to the external capsule. The primary difference is that area 36 of the 2 inbred strains has a generally less organized look than in the F1. For example, in the F1, layer II and layer III cells often form lines perpendicular to the pial surface, but this rarely happens in the inbred strains. Also, layer V does not show the typical size gradient. In the 129P3/J, there are smaller cells mixed in with the typical larger pyramids in deep layer V (Fig. 13*B*). In the C57BL6/J, very large pyramids appear in superficial V along with the typical small pyramids (Fig. 13*C*). Layer V of both inbred strains exhibits randomly placed cell-sparse patches. Another difference is that although all 3 strains have at least a narrow layer between III and V that contains granular cells, the dysgranular layer IV is more prominent in the F1 strain. Although there is a similar look, the layer containing granular cells is narrower in the inbred strains. Finally, the cortical depth of area 36 is less in the inbred strains. This could in part be due to a narrower layer VI.

Area 35 also exhibits strain differences. Perhaps the most salient differences are in the sizes of layer V pyramids. In the F1 mouse, area 35 layer V exhibits a size gradient that is clear though less prominent than in area 36. In the inbred strains, layer V of area 35 does not exhibit the typical size gradient. Another difference is that layers II–III of the inbred strains rarely show the lines of cells evident in area 36 layer II–III of the F1.

At midrostrocaudal levels, the cortical depth is roughly similar across strains and the packing density is also similar (Fig. 13, right panels). Both inbred strains continue to have a highly disorganized look as compared with the F1. In area 36 of the F1 mouse, the cells in layer II still tend to be organized in lines, layer V shows the size gradient, cells in layers II–III are

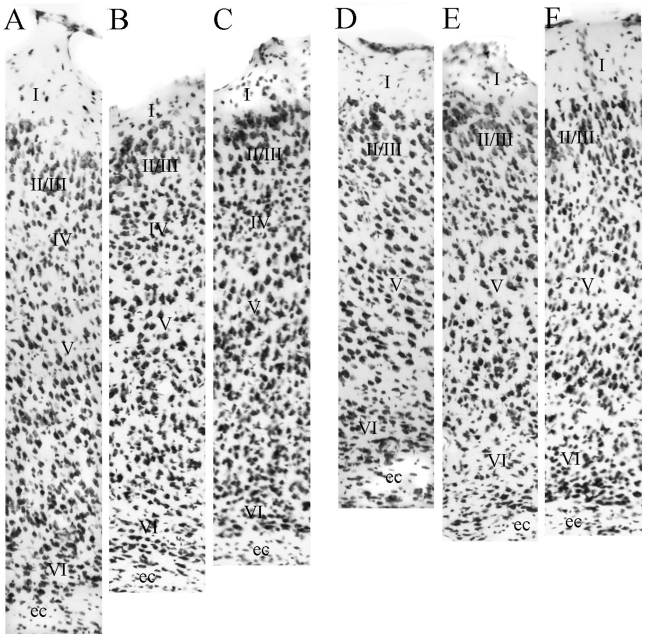

Figure 13. Photomicrographs comparing cortical layers of PER areas area 36 and 35 across strains. Shown are cortical layers for area 36 (*A–C*) and area 35 (*D–F*) for the F1 (*A* and *D*), the C57BL6/J, (*B* and *E*), and 129P3/J (*C* and *F*) mouse strains. The tissue was stained for Nissl material. Scale bar = 100 μm.

more densely packed and sometimes darker than in layer V, and there is an observable layer IV. None of these features is reliable in the inbred mice. In area 35 of the F1 mouse, the cells in layer II still tend to be organized in lines, but this is not the case in either inbred strain. Again, neither inbred strain shows the typical layer V size gradient, but the 129P3/J layer V has a bilaminate look such that the superficial sublayer contains smaller pyramids than the deep sublayer.

Caudal PER in the F1 mouse exhibits a staining intensity that is similar across all cellular layers, and the packing density is slightly higher than more rostral levels. This is true of the inbred strains, as well, but other features are different. Layer I is narrower in the inbred strains. Again, the overall appearance of area 36 is of a less organized agranular cortex. In the 129P3/J, cells tend to be larger and less densely packed. In the 129P3/J and the C57BL6/J, there are cell-sparse areas in layer V and no size gradient.

Although area 35 is agranular in all 3 strains, area 35 of the F1 has a more differentiated laminar appearance than area 35 of the inbred strains. Cells in area 35 layers II and III of the 129P3/J are more heterogeneous in packing, staining, and shape contributing to the disorganized look. Layer V is narrow and disorganized with cell-sparse patches and no size gradient. Area 35 layer V of the C57BL6/J mouse also has a disorganized look in that there is no size gradient and the cells vary widely in shape and orientation.

Strain differences are also apparent in the POR. The cortical depth of the 129P3/J mouse is shallower in both PORd and PORv (Fig. 14*D*,*F*). In the F1 mouse, the POR is located dorsal to the rhinal fissure, which is relatively prominent at rostral levels. Layer II of PORd has small round dark cells that have a patchy organization. Layer IV is dysgranular in the F1 mouse (Fig. 14*A*), but there is little evidence of a granular layer in the 2 inbred strains. Layer V is broad and exhibits a rough size gradient. There tends to be a cell-sparse gap between V and VI. Layer VI contains medium sized, moderately darkly staining, densely packed, round cells. In general, the region has a strong radial look in the F1 mouse. The PORd of the inbred strains lacks this radial appearance, though the region is similar in some of the details. In the C57BL6/J, cortical depth is less, there is no cell-sparse area between V and VI, and layer VI is less apparent. In the 129P3/J, layer V exhibits a bilaminate look in which the superficial cells tend to be smaller and deep cells tend to be larger. Again, there is no cell-sparse gap between layers V and VI. In the inbred strains, the cortex is dysgranular at best. At rostral levels, the rhinal fissure is shallower in the inbred strains as compared with the F1.

In PORv of the F1 mouse, layer I is broad and contains some ectopic layer II cells. Layer II cells are light, medium-sized, and round or oval. Cells in layer III are similar but tend to be radially oriented. Layer V exhibits a size gradient. Cells in the F1 mouse are more densely packed across all layers as compared with the inbred strains, most likely resulting in a higher total number of cells. In the inbred strains, layer II shows the ectopic cells near the border with entorhinal cortex, but they are less prominent than in the F1 mouse. The cortex lacks the radial appearance of the F1 mouse, and the cortical depth tends to be narrower.

Discussion

The general architecture of the mouse neocortex has been previously described (e.g., Rose 1929; Caviness 1975), but a detailed cytoarchitectonic analysis of the PER is not available, and none of the historical studies of the mouse cortical architecture identified a homolog of the POR in the rat brain (Burwell et al. 1995). We have analyzed the cytoarchitecture, myeloarchitecture, and histochemistry for the cortical regions located dorsal to the entorhinal cortex in the mouse brain (Fig. 3). Our analysis indicated that there is a region in the mouse brain caudal to the PER that is the homolog of the POR in the rat. Based on our analysis, we identified borders and subdivisions for the PER and POR regions in the mouse brain.

To summarize our findings, the rostral PER border with insular cortex is at the caudal limit of the claustrum, consistent with the placement of insular cortex proposed by Caviness (1975). The ventral and caudal borders with the entorhinal cortex are consistent with those proposed by van Groen (2001) for the mouse and by Insausti et al. (1997) for the rat. As in the rat, the caudal region associated with the rhinal fissure can be differentiated cytoarchitectonically and histochemically. Because the area exhibits similarities to the POR in the rat, we propose that this region also be termed the POR in the mouse. The border between the PER and POR is located at the caudal end of the angular bundle. Both the PER and POR are limited dorsally by temporal cortical regions as defined by others, for example, the temporal association area (Hof et al. 2000; Paxinos and Franklin 2001). Based on cytoarchitectonic and histochemical criteria, both the PER and POR were further subdivided. The PER was divided into areas 35 and 36. The POR was parcellated into dorsal (PORd) and ventral (PORv) subdivisions.

Nomenclature

Our designation of regional borders and subdivisions was informed by an earlier study of the same regions conducted in the rat (Burwell 2001), and that study was informed by comparisons with studies conducted in nonhuman primates

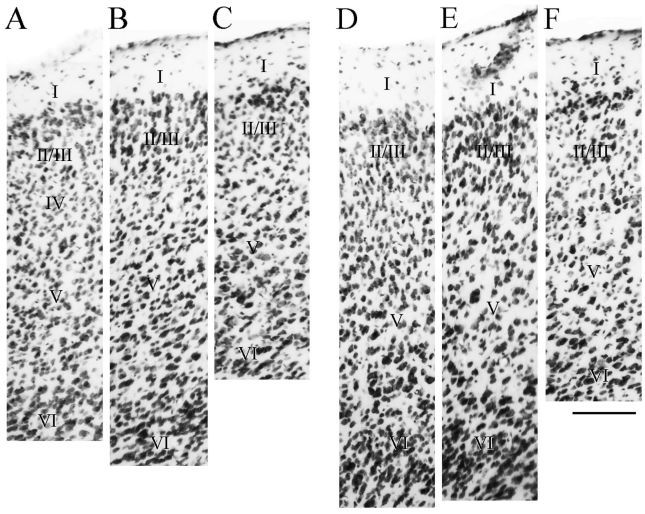

Figure 14. Photomicrographs comparing cortical layers of areas area 36 and POR across strains. Shown are cortical layers PORd (*A–C*) and PORv (*D–F*) for the F1 (*A* and *D*), the C57BL6/J, (*B* and *E*), and 129P3/J (*C* and *F*) mouse strains. Note that for PORd, only F1 has a clear, though dysgranular, layer IV. Scale bar = 100 μm.

(Burwell et al. 1995). In the rat brain, staining for heavy metals using the Timm's method was particularly useful in determining borders for the PER and POR. Material from the mouse brain prepared using the same methods yielded highly similar patterns of staining for heavy metals. Heavy metal staining patterns were also highly similar across all 3 mouse strains, which facilitated cross-strain comparisons.

Rose (1929) previously divided these regions into area perirhinalis and area ectorhinalis, a terminology also adopted in some modern stereotaxic atlases of the mouse brain (Hof et al. 2000; Dong 2008; Franklin and Paxinos 2008; Paxinos and Watson 2010). Caviness (1975) utilized Brodmann (1909) nomenclature, subdividing the PER into areas 35 and 36. Based on similarities between the rat and mouse brains in structural and histochemical features, we propose that the nomenclature we and others have used for the PER of rats and monkeys and the POR of rats be applied to the cortical regions associated with the rhinal fissure in the mouse. Accordingly, the PER comprises areas 35 and 36 and is bordered caudally by the POR, the homolog of the primate parahippocampal cortex (Burwell et al. 1995; Burwell 2001). This nomenclature, commonly employed for rats, has already been used for the mouse (van Groen 2001; Witter 2010), and we recommend its use in future editions of stereotaxic atlases of the mouse brain. Employing nomenclature similar to that used in other species, when possible, facilitates the use of rodent models of human cognition and neuropathology.

Comparisons across Strains

The initial analyses were carried out in first-generation hybrid mice, but detailed comparisons with the parent strains were included. The first-generation hybrid mouse was chosen for primary analysis for several reasons. In our own material, the PER and POR were better differentiated in the F1 brain, which facilitated the identification of borders. In addition, F1 hybrid mice tend to be better at cognitive tasks than inbred mouse strains. For example, in a study of 12 inbred strains and 7 different F1 hybrid lines, the F1 lines outperformed the inbred strains on spatial learning in the Morris water maze (Owen et al. 1997). To give another example, we found that F1 hybrid mice could learn a complex discrimination task, but the parent strains could not (Casten et al. 2011). Thus, our data support and extend existing recommendations about appropriate genetic background in neuroscience studies using mutant and transgenic mice (Silva et al. 1997). Of the available inbred mouse strains, the C57BL/6 and 129/J strains are likely the most widely used and are the recommended background for F1 lines (Silva et al. 1997). In this study, we made direct comparisons between these 2 inbred strains and the F1. By providing cytoarchitectonic and histochemical information on the F1 mouse and making comparisons to the parent strains, we hope to facilitate the use of F1 hybrid models in neuroscience research.

In general, we found that the cortex of the F1 mice exhibited more highly differentiated laminar patterns and had a more radial appearance as compared with the cortex of the inbred strains. In the 129P3/J and the C57BL6/J, both the PER and POR had a less radial look overall. This feature was particularly evident in layers II–III of the PER. In the F1, the cells in layers II–III tended to form lines, but this was rarely seen in the inbred strains. Additionally, area 36 and PORd in the inbred animals have fewer granule cells mixed in between layers III and V. Whereas these regions could be termed dysgranular cortex in the F1, they are better described as agranular cortices in the inbred animals. Layer V of the inbred mice was characterized by cell-sparse pockets, especially in the C57BL6/J, and layer V pyramidal cells tended not to show the typical size gradient. The cortical depth was shallower, overall, in the inbred strains.

Comparisons with Available Mouse Stereotaxic Atlases

Our borders and descriptions have some similarities and some differences with available atlases of the mouse brain. In some cases, nomenclature is the primary difference, but in others both borders and nomenclature differ. Most atlases use the coronal plane, and we have provided some basic information about the strains, subjects, and parametrics for our study and available atlases (Table 1). Franklin and Paxinos (2008) designate area 35 as perirhinal (PRh) and area 36 as ectorhinal (ECT). There is no designation of the postrhinal cortex. Rather, PRh and ECT cortices extend caudally past the angular bundle. The borders of these regions appear to have been identified relative to the rhinal sulcus and not according to any cytoarchitectonic or chemoarchitectonic features. Thus, at some levels, area 35 is misidentified as part of entorhinal cortex. At the angular bundle, PRh designates the lateral portion of entorhinal cortex and ECT designates what we have termed PORv. The 2 regions continue caudally for about half a millimeter until only a narrow region of cortex is designated as either PRh, for example, at bregma –4.84 or ECT at bregma –5.02. Paxinos and Watson (2010) chemoarchitectonic atlas does not include the POR and also misidentifies the border between the perirhinal and entorhinal cortices at multiple levels. The fundus and banks of the rhinal sulcus were identified as PRh, even at caudal levels where the rhinal sulcus is clearly occupied by entorhinal cortex. This atlas also presents material prepared in the sagittal plane, including a section at the same level shown in Figure 11. At 2.6 mm lateral to the midline, the parvalbumin sparse PORv is misidentified as

Table 1
Comparisons of subjects with those used in published atlases

Study or atlas	Strain	Age (weeks)	Weight (g)	β-λ (mm)	Nomenclature
Present study	F1 hybrid	19	26	4.69	36/35, PORd/PORv
	F1 hybrid	19	28	4.89	
	F1 hybrid	17	36	4.59	
	F1 hybrid	22	34	4.45	
	F1 hybrid	21	40	4.46	
Franklin and Paxinos (2008)	C57BL6	12	26–30	4.40	ECT/PER, ECT/PER
Paxinos and Watson (2010)	C57BL6	*	26	4.40	ECT/PER, ECT/PER
Hof et al. (2000)	C57BL6	15.7	28.7	~4.20	ECT/PER, ECT/PER
Hof et al. (2000)	SV129	21.4	29	~5.00	ECT/PER, ECT/PER
Slotnick and Leonard (1975)	Albino CF1	6–14	22–55	3.80	Not designated
Dong (2008)	C57BL6	8	25.2	~4.20	ECT/PER, ECT/PER

Note: All subjects were male. *, Data not available. The use of "~" for the distance between lambda and bregma indicates that we estimated from the data available. Under nomenclature, we provided designations in this format: rostral dorsal/rostral ventral, caudal dorsal/caudal ventral. Abbreviations: 35, area 35; 36, area 36; ECT, ectorhinal; PER; perirhinal; PORd, dorsal postrhinal cortex; PORv, ventral postrhinal cortex.

retrosplenial cortex. An older atlas also shows both coronal and sagittal planes (Slotnick and Leonard 1975). However, cortical borders are not delineated for these regions, and the sagittal planes do not include a level that shows the POR.

Although the nomenclature differs, our borders are very similar to those described in the Hof et al. (2000) atlas of the parent strains used for our F1 hybrid mouse shown in the coronal plane. Again, the terms PRh and ECT are used, and the POR is not defined as a separate region. At the level of the angular bundle, PRh corresponds to PORv and ECT corresponds to PORd. At more caudal levels, ECT is roughly equivalent to the combined PORv and PORd, although the border is slightly lower than we have placed it for PORd. Our borders are also similar to those of Dong (2008), although, again, that atlas uses the older terminology. In general, the perirhinal area corresponds to area 35 and the ectorhinal area corresponds to area 36. Just beyond the angular bundle, at about −4.38 mm relative to bregma, the perirhinal area corresponds to PORv and the ectorhinal area corresponds to PORd. More caudally, the ectorhinal area includes what we would designate as the combined PORv and PORd. In the sagittal sections, a narrow band dorsally adjacent to entorhinal cortex is labeled ectorhinal cortex. The dorsally and rostrally adjacent area is labeled as visual cortex, but this is most likely not the case as the laminar structure lacks a clear layer IV. At the level of 3.125 mm lateral to the midline in the sagittal plane, the parasubiculum is misidentified as ectorhinal cortex, and the dorsally adjacent region is misidentified as visual cortex. Based on cytoarchitectonic and histochemical criteria, PORv is certainly located dorsally adjacent to the parasubiculum (Fig. 11).

None of the published atlases have recognized the definition of the POR, which is now well established in the rat (Burwell et al. 1995; Naber et al. 1996, 1997, 2001; Witter et al. 2000; van Groen 2001; Burwell and Witter 2002, 2010; Witter and Amaral 2004). This is surprising, given that there are now also many studies in rodents, nonhuman primates, and humans showing functional dissociations between the perirhinal and postrhinal/parahippocampal cortex.

Comparisons with the Rat

Borders and subdivisions for the PER and POR in the F1 mouse, as described here, are similar to those for the rat (Burwell 2001), with the exception that we did not further subdivide areas 35 and 36 in the mouse brain. Otherwise, we have used the same nomenclature. A number of signature features were similar across the rat and the mouse. As in the rat, area 35 stains very lightly for parvalbumin, but staining is noticeably darker for area 36 (Burwell et al. 1995). In addition, the transition from insular cortex to the PER in the F1 mouse brain could be identified by the disappearance of the claustrum underlying the insular cortex and the appearance of a more homogenous look to the perirhinal region. Layer II of area 36 had a patchy organization, and the region exhibited a dysgranular look. Layer V in both areas 36 and 35 was characterized by the typical size gradient such that superficial pyramids were smaller than deep pyramids. The deep layer V pyramids in area 35 exhibited the heart-shaped appearance observed in the rat, though this feature was not as prominent in the mouse.

The POR of the mouse also shares some signature features with that of the rat. The transition to POR from PER occurs at the caudal limit of the angular bundle in both species. The transition is marked by ectopic layer II cells in layer I of PORv near the border with the ventrally adjacent entorhinal cortex. As in the rat, PORv stains very lightly for parvalbumin while PORd stains more darkly. In addition, PORd is dysgranular cortex, although the granular layer is better differentiated in the rat. As in the rat brain, the POR in the mouse brain is roughly similar to the caudal portion of what has been designated previously as perirhinal and ectorhinal cortices (Hof et al. 2000; Paxinos and Franklin 2001), with PORd corresponding roughly to caudal ectorhinal cortex and PORv corresponding roughly to caudal perirhinal cortex.

Conclusions

The PER and the POR/parahippocampal cortices are receiving more emphasis in neuroscientific research on memory (Bucci and Burwell 2004; de Curtis and Pare 2004; Squire et al. 2004; Aggleton and Brown 2005; Bussey et al. 2005; Eacott and Gaffan 2005; Murray et al. 2005; Buckley and Gaffan 2006), but we know very little about these regions in the mouse brain. Here, we have identified the PER and POR in the mouse brain and have described the borders, cytoarchitecture, and histochemistry in an F1 mouse, the B6129PF/J1 line. The PER was subdivided into areas 36 and 35, and the POR was subdivided into dorsal and ventral subdivisions. Certain signature features observed in the PER and POR of the rat brain were also present in the F1 mouse brain. These features informed our placement of the borders and choice of terminology. Comparisons between the 129P3/J and the C57BL6/J inbred strains and the F1 line suggested that these regions are better differentiated in the F1. Because behavioral phenotypes are more generalizable across F1 lines of mice, our findings support the view that the use of first-generation hybrid mice is optimal for studies of the neural bases of memory and of hippocampal-dependent functions.

Funding

National Institute of Mental Health R01 MH60284 and DARPA N66001-10-C-2010 (to R.D.B.).

Notes

We would like to acknowledge Ray D. Beck for his help editing an earlier draft of this manuscript. *Conflict of Interest*: None declared.

References

Aggleton JP, Brown MW. 2005. Contrasting hippocampal and perirhinal cortex function using immediate early gene imaging. Q J Exp Psychol B. 58:218–233.

Amaral DG, Insausti R, Cowan WM. 1987. The entorhinal cortex of the monkey: I. Cytoarchitectonic organization. J CompNeurol. 264:326–355.

Brodmann K. 1909. Vergleichende Lokalisationslehre der Grosshirnrinde in ihren Prinzipien dargestellt auf Grund des Zellenbaues. Leipzig (Germany): Barth.

Bucci DJ, Burwell RD. 2004. Deficits in attentional orienting following damage to the perirhinal or postrhinal cortices. Behav Neurosci. 118:1117–1122.

Buckley MJ, Gaffan D. 2006. Perirhinal cortical contributions to object perception. Trends Cogn Sci. 10:100–107.

Burwell RD. 2001. The perirhinal and postrhinal cortices of the rat: borders and cytoarchitecture. J Comp Neurol. 437:17–41.

Burwell RD, Amaral DG. 1998a. Cortical afferents of the perirhinal, postrhinal, and entorhinal cortices. J Comp Neurol. 398:179–205.

Burwell RD, Amaral DG. 1998b. Perirhinal and postrhinal cortices of the rat: interconnectivity and connections with the entorhinal cortex. J Comp Neurol. 391:293–321.

Burwell RD, Witter MP. 2002. Basic anatomy of the parahippocampal region in monkeys and rats. In: Witter MP, Wouterlood FG, editors. The parahippocampal region, organization and role in cognitive functions. London: Oxford University Press.

Burwell RD, Witter MP, Amaral DG. 1995. The perirhinal and postrhinal cortices of the rat: a review of the neuroanatomical literature and comparison with findings from the monkey brain. Hippocampus. 5:390–408.

Bussey TJ, Saksida LM, Murray EA. 2005. The perceptual-mnemonic/feature conjunction model of perirhinal cortex function. Q J Exp Psychol B. 58:269–282.

Casten KS, Gray AC, Burwell RD. 2011. Discrimination learning and attentional set formation in a mouse model of Fragile X. Behav Neurosci. 125:473–479.

Caviness VS. 1975. Architectonic map of neocortex of the normal mouse. J Comp Neurol. 164:247–264.

de Curtis M, Pare D. 2004. The rhinal cortices: a wall of inhibition between the neocortex and the hippocampus. Prog Neurobiol. 74:101–110.

Dong H-W. 2008. The Allen reference atlas: a digital brain atlas of C57Black/6J male mouse. Hoboken (NJ): Wiley.

Eacott MJ, Gaffan EA. 2005. The roles of perirhinal cortex, postrhinal cortex, and the fornix in memory for objects, contexts, and events in the rat. Q J Exp Psychol B. 58:202–217.

Eichenbaum H. 2000. A cortical-hippocampal system for declarative memory. Nat Rev Neurosci. 1:41–50.

Estill SJ, Fay K, Garcia JA. 2001. Statistical parameters in behavioral tasks and implications for sample size of C57BL/6J: 129S6/SvEvTac mixed strain mice. Transgenic Res. 10:157–175.

Franklin KBJ, Paxinos G. 1997. The mouse brain in stereotaxic coordinates. San Diego (CA): Academic Press.

Franklin KBJ, Paxinos G. 2008. The mouse brain in stereotaxic coordinates. New York: Academic Press.

Gass P, Wolfer DP, Balschun D, Rudolph D, Frey U, Lipp HP, Schutz G. 1998. Deficits in memory tasks of mice with CREB mutations depend on gene dosage. Learn Mem. 5:274–288.

Graves L, Dalvi A, Lucki I, Blendy JA, Abel T. 2002. Behavioral analysis of CREB alpha Delta mutation on a B6/129 F1 hybrid background. Hippocampus. 12:18–26.

Hedreen JC, Bacon SJ, Price DL. 1985. A modified histochemical technique to visualize acetylcholinersterase-containing Axons. J Histochem Cytochem. 33:134–140.

Hof P, Young W, Bloom F, Belichenko P, Celio M. 2000. Comparative cytoarchitectonic atlas of the C57BL6 and 129 Sv mouse brains. New York: Elsevier.

Hyde LA, Hoplight BJ, Denenberg VH. 1998. Water version of the radial-arm maze: learning in three inbred strains of mice. Brain Res. 785:236–244.

Insausti R, Herrero MT, Witter MP. 1997. Entorhinal cortex of the rat: cytoarchitectonic subdivisions and the origin and distribution of cortical efferents. Hippocampus. 7:146–183.

Kelly MA, Rubinstein M, Phillips TJ, Lessov CN, Burkhart-Kasch S, Zhang G, Bunzow JR, Fang Y, Gerhardt GA, Grandy DK, et al. 1998. Locomotor activity in D2 dopamine receptor-deficient mice is determined by gene dosage, genetic background, and developmental adaptations. J Neurosci. 18:3470–3479.

Lipp HP, Wolfer DP. 2003. Genetic background problems in the analysis of cognitive and neuronal changes in genetically modified mice. Clin Neurosci Res. 3:223–231.

Mizumori SJ, Rosenzweig MR, Kermisch MG. 1982. Failure of mice to demonstrate spatial memory in the radial maze. Behav Neural Biol. 35:33–45.

Montkowski A, Poettig M, Mederer A, Holsboer F. 1997. Behavioral performance in three substrains of mouse strain 129. Brain Res. 762:12–18.

Murray EA, Bussey TJ, Hampton RR, Saksida LM. 2000. The parahippocampal region and object identification. Ann N Y Acad Sci. 911:166–174.

Murray EA, Graham KS, Gaffan D. 2005. Perirhinal cortex and its neighbours in the medial temporal lobe: contributions to memory and perception. Q J Exp Psychol B. 58:378–396.

Naber PA, Caballero-Bleda M, Jorritsma-Byham B, Witter MP. 1997. Parallel input to the hippocampal memory system through peri- and postrhinal cortices. Neuroreport. 8:2617–2621.

Naber PA, Caballero-Bleda M, Witter MP. 1996. Perirhinal and postrhinal cortex innervate different parts of entorhinal cortex: indication for segregated information processing in the hippocampal system. Eur J Neurosci. (Suppl 9):100.

Naber PA, Witter MP, Lopes da Silva FH. 2001. Evidence for a direct projection from the postrhinal cortex to the subiculum in the rat. Hippocampus. 11:105–117.

Owen EH, Logue SF, Rasmussen DL, Wehner JM. 1997. Assessment of learning by the Morris water task and fear in inbred mouse strains and F1 hybrids: implications of genetic background for single gene mutations and quantitative trait loci analyses. Neurosci. 80:1087–1099.

Paxinos G, Franklin KBJ. 2001. The mouse brain in stereotaxic coordinates. New York: Elsevier.

Paxinos G, Watson C. 2010. Chemoarchitectonic atlas of the mouse brain. London: Academic press.

Quinn B, Graybiel AM. 1994. Myeloarchitectonics of the primate caudate-putamen. In: Percheron G, McKenzie JS, Férger J, editors. The basal ganglia IV: new ideas and data on structure and function. New York: Plenum Press. p. 35–41.

Rose M. 1929. Cytoarchitektonischer atlas der Groshirnrinde der Maus. J Psychol Neurol. 40:1–32.

Schmued LC. 1990. A rapid, sensitve histochemical stain for myelin in frozen brain sections. J Histochem Cytochem. 38:717–720.

Schwegler H, Crusio WE. 1995. Correlations between radial-maze learning and structural variations of septum and hippocampus in rodents. Behav Brain Res. 67:29–41.

Schwegler H, Lipp H-P. 1983. Hereditary covariations of neuronal circuitry and behavior: correlations between the proportions of hippocampal synaptic fields in the regio inferior and two-way avoidance in mice and rats. Behav Brain Res. 7:1–39.

Silva AJ, Simpson EM, Takahashi JS, Lipp HP, Nakanishi S, Wehner JM, Giese KP, Tully T, Abel T, Chapman PF, et al. 1997. Mutant mice and neuroscience: recommendations concerning genetic control. Neuron. 19:755–759.

Simpson EM, Linder CC, Sargent EE, Davisson MT, Mobraaten LE, Sharp JJ. 1997. Genetic variation among 129 substrains and its importance for targeted mutagenesis in mice. Nat Genet. 16:19–27.

Slotnick BM, Leonard CM. 1975. A stereotaxic atlas of the albino mouse forebrain. Rockville (MD); Washington: U.S. Dept. of Health, Education, and Welfare, Public Health Service, Alcohol, Drug Abuse, and Mental Health Administration.

Sloviter RS. 1982. A simplified Timm stain procedure compatible with formaldehyde fixation and routine paraffin embedding of rat brain. Brain Res Bull. 8:771–774.
Squire LR, Stark CE, Clark RE. 2004. The medial temporal lobe. Annu Rev Neurosci. 27:279–306.
Suzuki WA, Amaral DG. 2003. Perirhinal and parahippocampal cortices of the macaque monkey: cytoarchitectonic and chemoarchitectonic organization. J Comp Neurol. 463:67–91.
Upchurch M, Wehner JM. 1988. Differences between inbred strains of mice in Morris water maze performance. Behav Genet. 18:55–68.
van Groen T. 2001. Entorhinal cortex of the mouse: cytoarchitectonical organization. Hippocampus. 11:397–407.
van Groen T, Kadish I, Wyss JM. 2002. Species differences in the projections from the entorhinal cortex to the hippocampus. Brain Res Bull. 57:553–556.
Van Hoesen GW, Pandya DN. 1975. Some connections of the entorhinal (area 28) and perirhinal (area 35) cortices of the rhesus monkey. I. Temporal lobe afferents. Brain Res. 95:1–24.
Voikar V, Koks S, Vasar E, Rauvala H. 2001. Strain and gender differences in the behavior of mouse lines commonly used in transgenic studies. Physiol Behav. 72:271–281.
Walters CL, Blendy JA. 2001. Different requirements for cAMP response element binding protein in positive and negative reinforcing properties of drugs of abuse. J Neurosci. 21:9438–9444.
Whishaw IQ, Tomie JA. 1996. Of mice and mazes: similarities between mice and rats on dry land but not water mazes. Physiol Behav. 60:1191–1197.
Willot JF. 1986. Effects of aging, hearing loss, and anatomical location on thresholds of inferior colliculus neurons in C57BL/6 and CBA mice. J Neurophysiol. 56:391–408.
Witter MP. 2010. Hippocampus. In: Watson C, editor. Mouse nervous system. London: Academic Press. p. 112–138.
Witter MP, Amaral DG. 2004. Hippocampal formation. In: Paxinos G, editor. The rat nervous system. 3 ed. San Diego (CA): Academic Press, Inc. p. 635–704.
Witter MP, Naber PA, van Haeften T, Machielsen WC, Rombouts SA, Barkhof F, Scheltens P, Lopes da Silva FH. 2000. Cortico-hippocampal communication by way of parallel parahippocampal-subicular pathways. Hippocampus. 10:398–410.
Wolfer DP, Lipp HP. 2000. Dissecting the behaviour of transgenic mice: is it the mutation, the genetic background, or the environment? Exp Physiol. 85:627–634.